Hindawi
Advances in Materials Science and Engineering
Volume 2018, Article ID 8214604, 9 pages
https://doi.org/10.1155/2018/8214604

Research Article

Shear Parameters of Rammed Earth Material: Results from Different Approaches

R. El-Nabouch,[1] Q.-B. Bui,[2] P. Perrotin,[1] and O. Plé[1]

[1]*Univ. Grenoble Alpes, Univ. Savoie Mont Blanc, CNRS, LOCIE, 73000 Chambery, France*
[2]*Sustainable Developments in Civil Engineering Research Group, Faculty of Civil Engineering, Ton Duc Thang University, Ho Chi Minh City, Vietnam*

Correspondence should be addressed to Q.-B. Bui; buiquocbao@tdtu.edu.vn

Received 16 June 2018; Accepted 14 August 2018; Published 17 October 2018

Academic Editor: Zbyšek Pavlík

Rammed earth (RE) is a construction material which is manufactured by compacting the soil in a formwork, in different layers. Several recent studies have investigated this material. The seismic performance of RE buildings is an important topic which needs to be carefully investigated. The complex numerical model seems a performant approach to investigate the seismic performance of a whole building. To correctly establish the model, the shear parameters of the material, which are the cohesion and the friction angle, should be identified. This paper first presents experimental studies on the shear parameters of RE through the direct shear tests, at two different scales. The differences of the results at different scales are analyzed. Then, the obtained experimental values are used in a numerical model to simulate the shear behavior of RE walls which are loaded by a constant vertical stress and pushed horizontally on the top. From the obtained results, the values for numerical models are recommended.

1. Introduction

Rammed earth is an ancient technique of construction where the wall is built by compacting the soil in a formwork, in different layers. Each earthen layer has thicknesses of about 10–15 cm. More details about this technique of construction are presented in [1, 2]. This material is recently experiencing a renewed interest because of its low embodied energy [3], its recycling ability, and a positive hygrothermal behavior which offers an attractive living comfort [4]. Figure 1 illustrates an example of a recent school in France constructed by RE material.

A nonnegligible number of studies on RE material are observed during the last decade, on different topics: mechanical characteristics [5–9], thermal and hygrothermal properties [4, 10], and durability [11, 12]. For the earthquake performance of RE structures, although several studies have explored this topic [13–16], different aspects still need to be investigated more thoroughly. In order to study the earthquake behavior of an entire RE structure, robust numerical models are a necessary approach. For the numerical modelling of RE material, two important shear parameters are the friction angle φ and the cohesion c. Due to the superposition of successive earthen layers during the manufacture of RE walls, two kinds of characteristics should be distinguished: characteristics of the earthen layers ("intralayer") and those of the interfaces between earthen layers ("interlayer") [17]. The first scope of the present study is to identify the relevant values of the friction angle φ and the cohesion c for both intralayers and interlayers. The characterization of these parameters is the first important step to create performant numerical models for the seismic evaluation of RE buildings.

Several previous studies in the literature tried to identify these two parameters but important dispersions in the obtained results were observed. Cheah et al. [18] performed triaxial tests on cement-stabilized RE specimens and obtained friction angles from 45° to 56°. Bui et al. [19] used analytical calculations for RE specimens and indirectly obtained for intralayers a friction angle of 51° and a cohesion of 0.1 f_c, where f_c is the compressive strength. Nowamooz and Chazallon [20] used finite elements modelling with the

Figure 1: A recent school in France using RE material, architect: V. Rigassi.

Barcelona model on small compacted soil specimens and identified a friction angle and a cohesion of 41° and 13.4 kPa, respectively. Bui et al. [17] used discrete elements modelling to identify c and φ; the identified friction angle was of 45–50° and the identified cohesion was of 100–150 kPa. Miccoli et al. [21, 22] identified numerical values of 30–45° for intralayer friction angles.

The experimental approach is a feasible way which provides "direct" values, while for the numerical approach, a calibration of the results is needed and the identified values are "indirect". The difficulty with RE material is that the representativeness of the tested specimens should be insured because of a high inhomogeneity of the material [6]. El-Nabouch et al. [23] present an experimental study on a full-scale direct shear test where the friction angle and the cohesion of the intralayers were of 37.3° and 30 kPa, respectively. The present paper first presents the results about the cohesion and the friction angle of RE intralayers and interlayers and obtains the following different scales: on standard direct shear tests (10 cm × 10 cm × 4 cm) and on the full-scale direct shear tests (50 cm × 50 cm × 45 cm). Then, the experimental results are used in a numerical model to simulate the behavior of two RE walls which were tested under a constant vertical stress and a horizontal force on the top of the wall. The results and recommendations will be presented.

2. Experimental Studies

2.1. Material Used. The earth used was provided by a RE manufacturer company, in the Rhône-Alpes region (France). This soil had been used to build numerous ancient RE buildings in this region. The grain size distribution of the earth is presented in Figure 2. The composition of the soil was analyzed by X-ray powder diffraction where the data were recorded on small fractions of specimens that were crushed before the analysis. The diffraction patterns were recorded with a Bruker D8 diffractometer. The result (shown in Figure 3) reveals the presence of quartz (72.6%), albite (15.1%), illite (11%), and trace of vermiculite (1.3%) [24]. The Proctor optimum water content is of 12% (by weight), determined following the French standard [25].

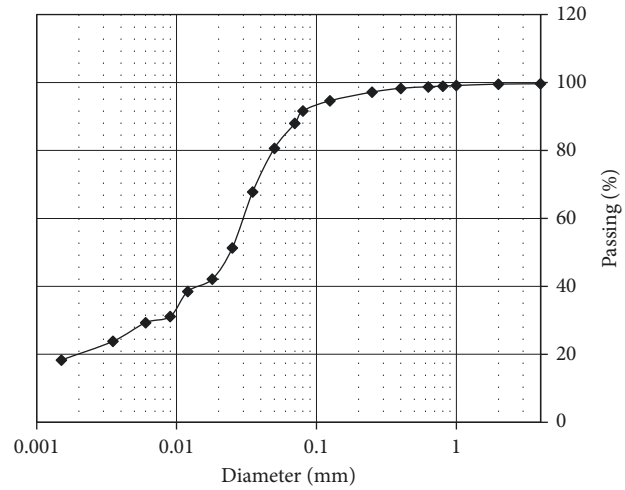

Figure 2: Grains size distribution of the earth used.

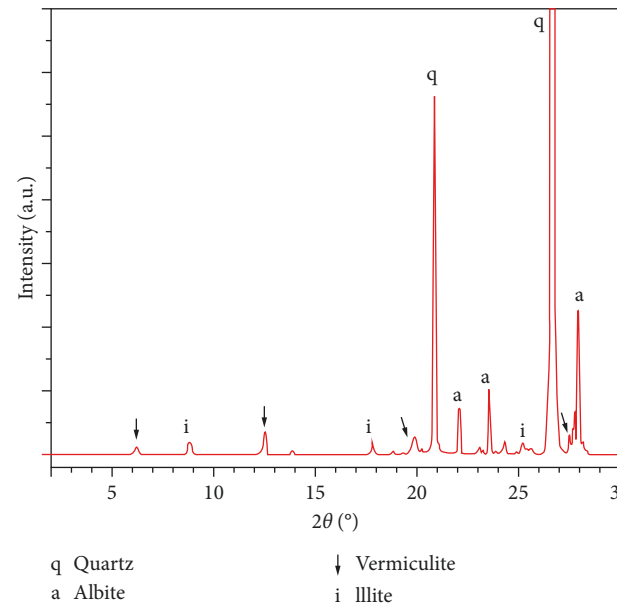

Figure 3: X-ray diffraction result of the used soil [24].

2.2. Standard Direct Shear Tests

2.2.1. Test Method. Casagrande's shear test is a classical test in soil mechanics [26]. The soil specimen is placed in a shear box that consists of two independent half boxes; the contact between the two half boxes is at the midheight of the specimen. A vertical confining stress is applied to the specimen, and the upper half boxes are pulled laterally (speed of 1.5 mm/min) until the specimen fails. Three tests (at three different vertical stresses) are carried out to determine c and φ following Mohr–Coulomb's theory.

In the present study, the standard shear box (dimensions of 10 cm × 10 cm × 4 cm), which is usually used to identify the friction angle and the cohesion of sand or soil, was also used to test RE specimens (Figure 4).

In soil mechanics, specimens are directly fabricated in the shear box. However for RE material, the representativeness of the specimens manufactured in "small" moulds (compared to in situ RE walls) is usually problematic. Indeed, manufacturing a representative RE specimen by a pneumatic rammer in a small box (10 cm × 10 cm × 4 cm) is not easy. That was why the authors decided to take specimens directly from a 1.5 m width × 1.5 m height × 0.25 m thickness RE wall, which will be presented in detail in the next section. The wall was manufactured in a steel formwork with plywood plates. The earth was compacted by a pneumatic rammer, at 12% of manufacturing water content (by weight) and in 12 earthen layers (with 12 cm thick for each layer). Preliminary Proctor tests showed that this water content was the optimum value for the compaction energy of the pneumatic rammer used. The wall was unmolded from its formwork after the manufacturing and then cured at laboratory ambient conditions (20°C and 60% relative humidity, RH) during two months.

The specimens for direct shear tests were taken after two months and at a quasi-dry state (less than 3% of moisture content, by weight). Firstly, earthen blocks (about 35 cm × 35 cm × 15 cm) were taken from the wall (Figure 5(a)). Then, a table saw was used to cut specimens into accurate dimensions (10 cm × 10 cm × 3.5 cm), enabling to fit the shear box (Figures 5(b) and 5(c)). Since Bui et al. [6], it has been well known that the density in a RE layer decreased from the top to the bottom. That was why specimens for the standard shear tests were taken at different positions in an earthen layer: at 1 cm from the top (Figure 5(b)) where the compaction was the most important (dry density measured of $1864 \pm 51\ \text{kg/m}^3$) and at the middle of the layer (Figure 5(c), dry density of $1703 \pm 45\ \text{kg/m}^3$). The specimens at the bottom, close to the interface, could not be extracted because they were too brittle. It is worth noting that due to the fragility of unstabilised RE material, special attentions must be paid to correctly cut the specimens without visible damage (for example, [27]).

2.2.2. Test Results. For each direct shear test, the maximum shear stress was noted and the experimental results giving the relationship between the shear stress τ and the normal stress σ are summarized in Figure 6. Firstly, note that the tests are consistent with Mohr–Coulomb's theory since the experimental results are on the same straight line (a correlation coefficient greater than 97%). Furthermore, the graph shows that, at a same vertical stress, the specimens from the upper part had a shear resistance greater than that of the lower part. This result is not surprising because the upper part—which is better compacted during the manufacturing—has a greater density and therefore has a strength which is greater than that of the lower part.

Following Mohr–Coulomb's theory, the relationship between the maximum shear stress and the normal stress is determined. The result is presented in Figure 6 for the case of the standard shear box. The apparent friction angle and the apparent cohesion were determined, giving, respectively, $\varphi = 44.1^\circ$ and $c = 264$ kPa for the specimens taken from the layers' upper parts, whereas $\varphi = 44.4^\circ$ and $c = 164$ kPa for the specimens taken for the layers' middle parts. It is interesting to note that the friction angles obtained were similar for the upper and middle parts of an earthen layer (about 44°). The main difference was the cohesion: the upper part had a more important cohesion (264 kPa), comparing to that of the middle part (164 kPa).

Figure 4: A standard direct shear test with a RE specimen inside the standard shear box.

2.3. Full-Scale Direct Shear Tests. In a recent study, El-Nabouch et al. [23] have carried out an experimental study on a full-scale shear box (50 cm × 50 cm × 45 cm height) to take into account the scale effects (Figure 7). The soil used and the manufacturing process were the same as that of the present study. Two types of shearing tests were performed: specimens sheared at the middle of layer (intralayer) and specimens sheared at the interface between the layers (interlayer). Due to the large size of the specimens, there was a high variation of the moisture content inside of the specimens, which was from 3% to 6%, depending on positions (on the surface or at interior).

First, a vertical load is applied on the top of the specimen (by the vertical actuator VA), and then, a horizontal load is applied by the horizontal actuator VH. The results (Figure 8) showed that the friction angle and the cohesion of the intralayers were of 37.3° and 31 kPa, respectively, and that of the interlayers were of 34.8° and 24 kPa, respectively.

2.4. Discussion. The results obtained show that, for a same scale of test, the friction angle does not vary significantly within a RE wall: between the upper part and the middle part in the case of standard shear box tests (about 44°) and

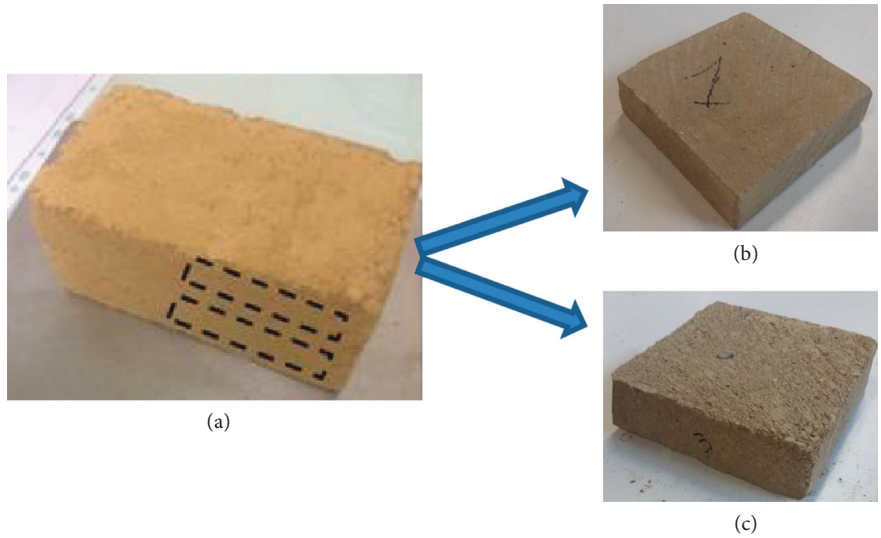

Figure 5: Location of the specimens inside one layer: upper (b) and middle (c) parts of the layer.

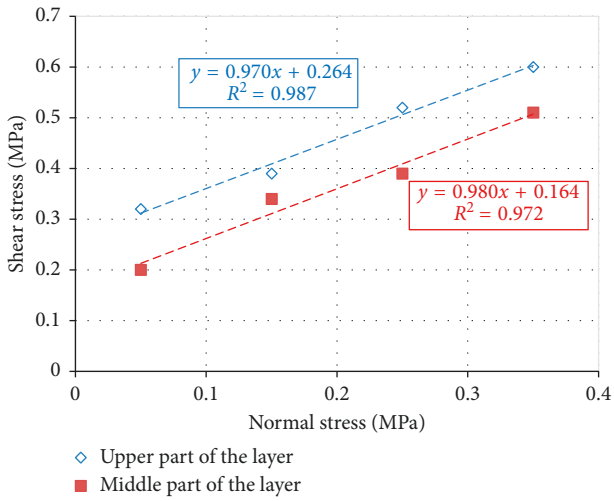

Figure 6: Results of standard direct shear tests.

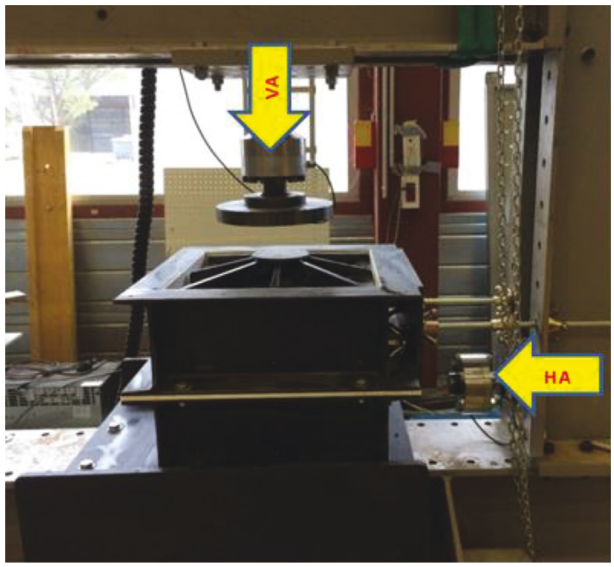

Figure 7: The full-scale shear box installed on the loading frame.

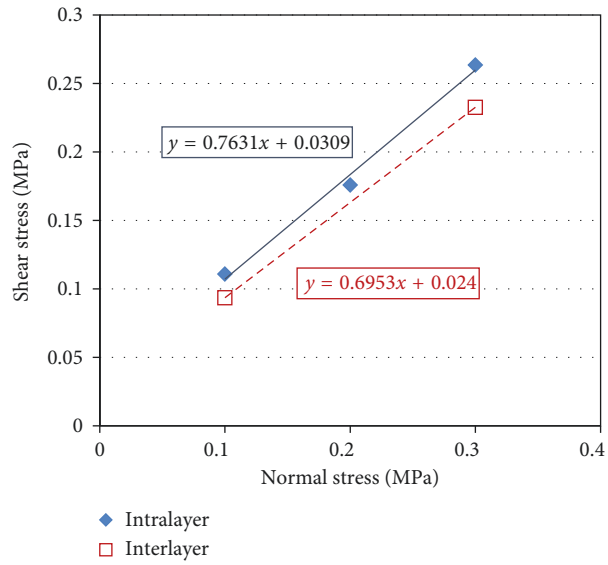

Figure 8: Results obtained from the full-scale shear box tests.

between the intralayer and the interlayer in the case of full-scale shear box tests (37.3° and 34.8°, respectively). It is suggested that the friction angle depends on the roughness of earth grains which is similar between the upper and middle parts of a layer. Besides the grain roughness, the density has also influence on the friction angle, which explains the slightly lower values of the interlayer friction angle, compared to that of the intralayer.

For the cohesion, the difference is clearer between the upper part and the middle part (264 and 164 kPa, respectively). It is suggested that, with a higher compactness, the dimensions of the micropores in the upper part are smaller than that of the middle part; the smaller micropores give a higher suction which provides higher cohesion and mechanical strength [7, 28]. This observation is also valid for the full-scale shear box tests where the interlayer cohesion is about 80% of the intralayer cohesion.

Another important observation is that the results obtained on the full-scale shear box are lower than that of the standard shear tests. Indeed, the shear tests at the midlayer on the standard box were conducted at a similar position with the intralayer shear tests on the full-scale box; for the standard box tests, the friction angle and the cohesion of the middle part are 44° and 164 kPa, respectively, while these parameters obtained on the full-scale box test are 37° and 31 kPa, respectively. The main differences between these two tests are the specimens' size and the moisture content. Indeed, it was observed that the moisture content was not homogeneous in the full-scale specimens and varied from 3% to 6%, depending on the positions, whereas the moisture content played a predominant role on the suction of earthen material which was the main source of the cohesion in earthen material [7, 8, 28, 29].

The influence of the moisture content is also probable because the cohesion obtained on intralayer full-scale specimens were relatively low (31 kPa). For comparison, following the formulas recommended in New Zealand Standard [30] or in [19], the cohesion would be 100–200 kPa for the RE in the present study; or following the values suggested in [22], the intralayer cohesion would be in the range from 132 to 264 kPa in the present study.

The low values of the cohesion and the friction angle obtained through the full-scale shear box are likely due to the effects of the moisture content, but also due to the size effects. Indeed, Flitti et al. [31] observed that when the moisture content increased (from 0 to 3%), the friction angle could decrease about 1° (for a friction angle of 40°). So, it can be suggested that the moisture may act as a lubricant which decreases the friction between the particles, but this phenomenon does not have enough effects to explain the low results obtained. This result confirms the nonnegligible role of the size effects.

From the results of intralayer and interlayer obtained on the full-scale box, the friction angle of the interlayer is 93% of the intralayer and the cohesion of the interlayer is 80% of the intralayer. This is an interesting result which serves for the numerical modelling.

3. Numerical Modelling of RE Shear Walls

For the numerical modelling, due to the simplicity, the earthen layers are usually assumed homogeneous and the interfaces are added between layers [17]. However, the above experimental results showed that there was a difference in the cohesions and the friction angles between the upper and middle parts of an earthen layer. So it is important to take the pertinent values for homogenized earthen layers (in numerical models) which represent the real inhomogeneous layers. On the contrary, it has already been observed that the most adapted values for a numerical model may sometimes be slightly different from the intrinsic characteristics of the material [32]. That was why a finite element (FE) model was built and simulated two horizontal loading tests in order to find the recommended values for the modelling of RE material.

3.1. Horizontal Loading Tests. Two walls (called wall A and wall B) were used for the numerical modelling of the present study. The walls having 1.5 m width × 1.5 m height × 0.5 m thickness (Figure 9) were manufactured with the same soil and the manufacturing process as the specimens presented above. The walls' moisture contents obtained after the test were 2.5–3% (i.e., the same as the specimens tested in the standard shear box).

The RE wall was directly built on a concrete beam. After the RE wall manufacturing, a second concrete beam was installed on the top of the RE wall, by applying a lime mortar. These walls were subjected to the pushover test which is a reliable approach to evaluate the walls' earthquake performance. First, vertical loads were applied on the top of the wall by means of two vertical actuators (VE1 and VE2 (Figure 9)). These loads corresponded to a vertical compressive stress of 0.3 MPa, which simulated the stress due to the vertical loads in a building (dead and live loads). Then, the horizontal pushing load was applied from a horizontal actuator (VH) with a displacement control (0.01 mm/s). The digital image correlation (DIC) technique was used to measure the displacements of the walls during the tests. In the DIC technique, the displacement fields are determined by comparing the images taken after and before loading (reference image). A professional camera with a resolution of 16 M pixels was used. The test was recorded by the camera, and the data processing was performed with the 7D software [33].

The bottom concrete beam was fixed to the steel frame by four steel brackets that could be mechanically adjusted (Figure 9). Another steel prop (*B* on Figure 9) was used as support to prevent the beam sliding when the top horizontal displacement is applied. The bottom concrete beam was also maintained by vertical tie rods (*T* on Figure 8) to avoid the beam rocking. Three displacement sensors M1 and M2 were installed to verify if there were any movement (vertical and horizontal) of the bottom concrete beam. The displacement sensor M3 was used to verify the accuracy of the results obtained from DIC.

Figure 10 shows the horizontal forces in function of the horizontal displacements on the top of both walls. These displacements were obtained from the DIC. Two walls tested exhibit similar initial stiffness and a nonbrittle behavior; the maximal horizontal load was 40–43 kN.

Figure 11 illustrates the crack propagation of wall A through the results of the major principal strains obtained from the DIC process. For the tested walls, three types of cracks were identified: first, a horizontal crack was observed at an interface between two earthen layers at the left-lower part of the wall. Second, inclined cracks which represent the diagonal compressive strut. These cracks appeared when the horizontal load reached about 80–85% of the maximal load. Third, the rocking of the walls at their base was also noted at the end of the tests (on the right side of the wall on Figure 11).

3.2. Numerical Modeling

3.2.1. Initial Considerations. The horizontal loading tests were modeled with Aster code [34] by using 3D solid

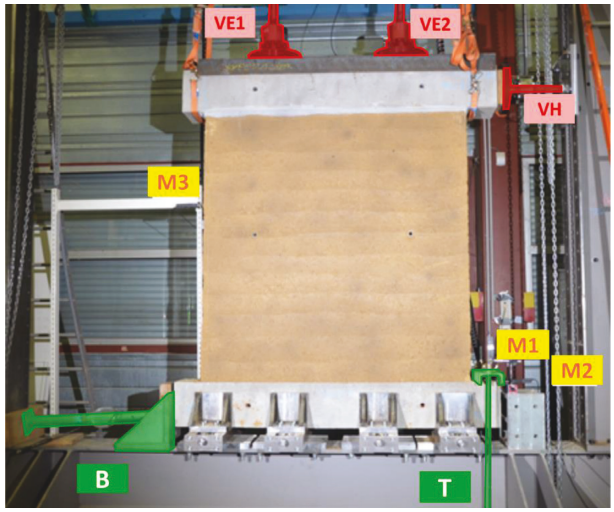

Figure 9: Test setup on a RE wall (1.5 m × 1.5 m × 0.25 m).

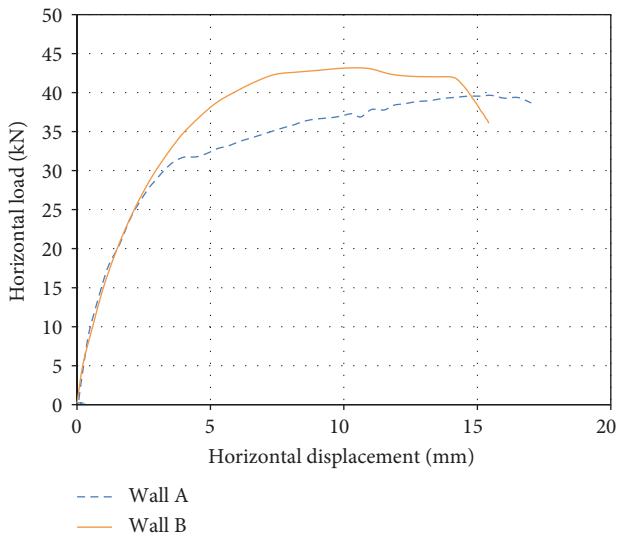

Figure 10: Horizontal forces on top of the wall in function of the top horizontal displacements.

elements. Aster is a FEM code, developed by Electricity of France. This code has different advanced options for the earthquake studies and was used to model different important and complex structures such as nuclear power plants. The initial aim of the authors of this paper is to first validate the numerical model at the wall scale and then apply for entire RE structures for further studies.

The well-known Drucker–Prager's model was chosen. In fact, Drucker–Prager's model does not directly use c and φ as parameters, but a conversion from Mohr–Coulomb' parameters is necessary. However, Drucker–Prager's model was used in the present study due to its robustness (working in 3D) and its simplicity by comparing to other advanced models. Drucker-Prager's yield criterion is written as follows:

$$F(\sigma, p) = \sigma_{eq} + \alpha I_1 - R(p) = 0, \quad (1)$$

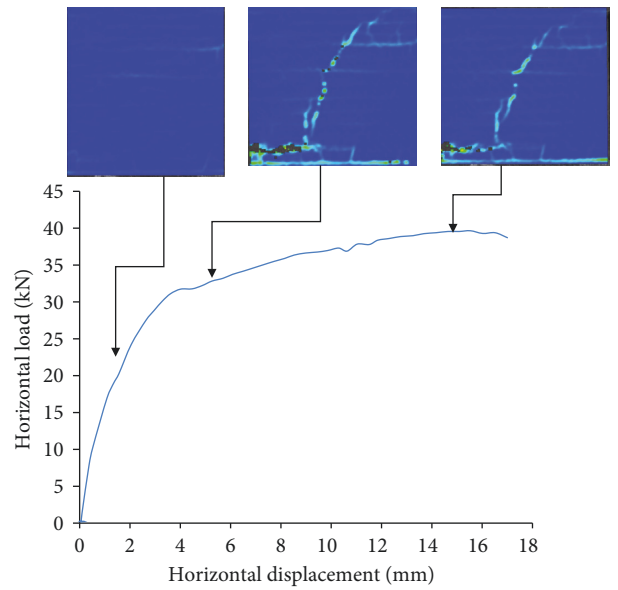

Figure 11: Evolution of cracking for the wall A in function of the horizontal displacement.

where $I_1 = \mathrm{tr}(\sigma)$ is the trace of the stress tensor, σ_{eq} is the second invariant of stress, and α is a function of the friction angle:

$$\alpha = \frac{2\sin\varphi}{3 - \sin\varphi}. \quad (2)$$

$R(p)$ is the value taken by the criterion for $\mathrm{tr}(\sigma) = 0$, a function of the cumulated plastic strain p. The variation of R with the material plasticization presents the hardening. The parabolic hardening is chosen for this model.

The parameter σ_y is written in the function of φ and the cohesion c:

$$\sigma_y = \frac{6c\cos\varphi}{3 - \sin\varphi}. \quad (3)$$

Figure 12 illustrates the geometry and the meshing. The wall was modeled with 12 layers of 11.4 cm each (named "intralayer") and thin layers of 1 cm (named "interlayer") between the earthen layers. Indeed, the role of the interlayers may not be predominant in the case of vertical loads but important in the cases where the interfaces are more solicited [17]. In the present study where the walls are subjected to horizontal loads, the effects of interlayers on the model might have a significant impact on the results. In fact, the interlayers represent the bottom part of an earthen layer where the soil was less compacted than the upper part, and consequently, its mechanical properties are lower. The thickness of the interlayers was chosen following observations by DIC during compression tests where the thickness of the weak layers (excessive displacements compared to other parts) was about 1 cm. Modelling these two layers is a simple way which enables to consider each intralayer and each interlayer with different parameters. Each intralayer

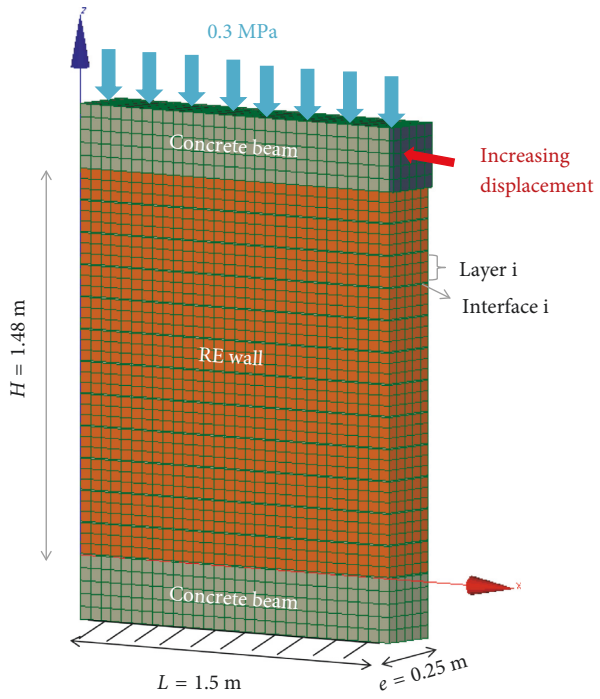

Figure 12: Geometry and boundary conditions of the numerical model.

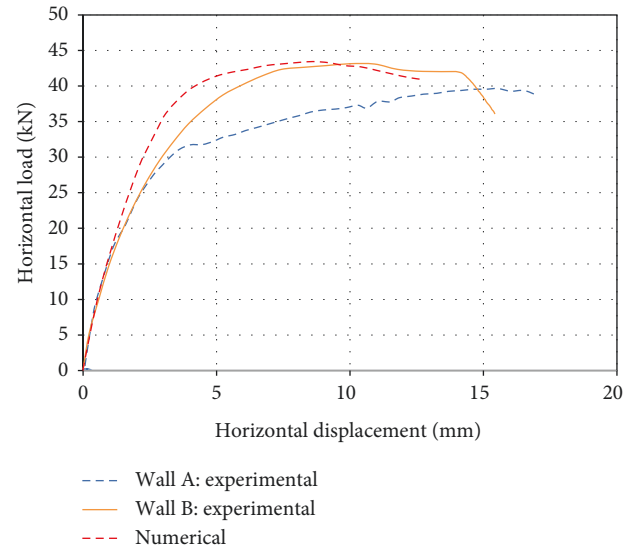

Figure 13: Numerical results for the cases of with and without interfaces.

and each interlayer are considered as homogeneous and isotropic. The bottom of the bottom concrete beam is considered as embedment.

3.2.2. Intralayer and Interlayer Characteristics. For the intralayers, Young's modulus was taken of 500 MPa that was measured by DIC during the vertical loading phase of the experiment, by using the vertical displacements at the walls' central part. Poisson's ratio was taken equal to 0.23, following the results of a previous study [7].

As mentioned above, the moisture content of the tested walls is similar to that of the specimens tested in the standard shear box, so the intralayer characteristics were taken following the results of the standard shear box. The interlayer characteristics were taken in percentage of the intralayer characteristics, as obtained on the full-scale shear box tests. Therefore, the intralayers were modeled with $\varphi_{\text{intra}} = 44^\circ$ and $c_{\text{intra}} = 164$ kPa, which are the values of the middle part of a layer because the numerical model considered each earthen layer as a homogeneous material. The interlayer friction angle was taken as 94% of the intralayer, corresponding to $\varphi_{\text{inter}} = 40^\circ$; the interlayer cohesion was taken as $c_{\text{inter}} = 130$ kPa which represented 80% of the intralayer cohesion.

3.2.3. Numerical Results and Discussions. The numerical results are illustrated in Figure 13. From this figure, the numerical model could reproduce the maximum force of the experiments, the experimental initial stiffness, and the global elastoplastic behavior. The experimental second slope before the maximal load was less well reproduced; this result is probably due to the limited number of parameters used in the Drucker–Prager model, compared to other more sophistical models which use more parameters [32].

Figure 14(a) illustrates the major principal strains for the model, which show the strain concentration at the left base of the RE wall on the diagonal line. The slight rocking at the right base is also observed. These strain concentrations correspond to the damages observed during experiments (Figure 14(b)).

If a pushover analysis following Eurocode 8 is carried out to assess the in-plane seismic performance of these walls by using the numerical curve of horizontal load-horizontal displacement (more details can be found in [13, 35]), the position of the numerical performance point will be close to the experimental performance point. This result means that the numerical model can provide satisfying results for the pushover analysis.

4. Conclusion

In the present paper, the shear parameters of RE material were first experimentally investigated by standard direct shear tests. For the standard direct shear tests, two types of specimens were tested: specimens taken at the upper parts of an earthen layer and specimens taken at the middle parts. The results obtained for the upper part were $\varphi_{\text{layer}} = 44^\circ$ and $c_{\text{layer}} = 264$ kPa, and for the lower part, they were $\varphi_{\text{layer}} = 44^\circ$ and $c_{\text{layer}} = 164$ kPa. The interesting finding was that the friction angles obtained for the upper and middle parts of an earthen layer were similar because of the similar roughness of earth grains and that the upper part had higher cohesion than the middle part due to a higher suction.

Then, the results obtained on a full-scale shear box were also presented to provide information about the interfaces between earthen layers. The results showed

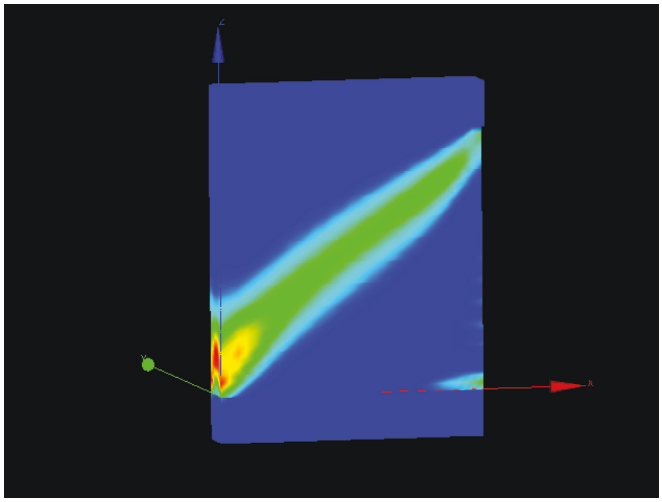

(a)

(b)

Figure 14: (a) Maximum principal strains in the numerical model; (b) wall damages.

that the interlayer friction angle was 93% of the intralayer and that the interlayer cohesion was 80% of the intralayer.

Finally, these experimental results were used for a numerical simulation of two RE walls subjected to horizontal loading tests. The numerical model could reproduce the maximum force of the experiments, the experimental initial stiffness, the global elastoplastic behavior, and the crack evolution during the experiments. These results showed the relevancy of the shear parameters used in the numerical model and that the model could be directly used for the pushover analysis on the seismic performance assessment of RE structures.

Data Availability

The data used to support the findings of this study are available from the corresponding author upon request.

Conflicts of Interest

The authors declare that they have no conflicts of interest.

Acknowledgments

This research is funded by the Vietnam National Foundation for Science and Technology Development (NAFOSTED) under grant number 107.01-2017.22. The authors wish also to thank the French National Research Agency (ANR) for the PRIMATERRE project (ANR-12-Villes et Bâtiments Durables) which supports the Ph.D. thesis of the first author [35]. L. Teytu, M. Jaffré, and the technical staffs from LOCIE (USMB) are warmly thanked for their precious collaboration.

References

[1] P. Walker, R. Keable, J. Martin, and V. Maniatidis, *Rammed Earth: Design and Construction Guidelines*, BRE Bookshop, Watford, UK, 2005.

[2] M. Hall, R. Lindsay, and M. Krayenhoff, *Modern Earth Buildings-Materials, Engineering, Constructions and Applications*, Woodhead Publishing, Sawston, UK, 2012.

[3] J. C. Morel, A. Mesbah, M. Oggero, and P. Walker, "Building houses with local materials: means to drastically reduce the environmental impact of construction," *Building and Environment*, vol. 36, no. 10, pp. 1119–1126, 2001.

[4] L. Soudani, A. Fabbri, J. C. Morel et al., "Assessment of the validity of some common assumptions in hygrothermal modeling of earth based materials," *Energy and Buildings*, vol. 116, pp. 498–511, 2016.

[5] C.T. S. Beckett, C. E. Augarde, D. Easton, and T. Easton, "Strength characterisation of soil-based construction materials," *Géotechnique*, vol. 68, no. 5, pp. 400–409, 2017.

[6] Q. B. Bui, J. C. Morel, S. Hans, and N. Meunier, "Compression behaviour of non-industrial materials in civil engineering by three scale experiments: the case of rammed earth," *Materials and Structures*, vol. 42, no. 8, pp. 1101–1116, 2009.

[7] Q. B. Bui, J. C. Morel, S. Hans, and P. Walker, "Effect of moisture content on the mechanical characteristics of rammed earth," *Construction and Building Materials*, vol. 54, pp. 163–169, 2014.

[8] F. Champiré, A. Fabbri, J.-C. Morel, H. Wong, and F. McGregor, "Impact of relative humidity on the mechanical behavior of compacted earth as a building material," *Construction and Building Materials*, vol. 110, pp. 70–78, 2016.

[9] V. Maniatidis and P. Walker, "Structural capacity of rammed earth in compression," *Journal of Materials in Civil Engineering*, vol. 20, no. 3, pp. 230–238, 2008.

[10] P. Taylor, R. J. Fuller, and M. B. Luther, "Energy use and thermal comfort in a rammed earth office building," *Energy and Buildings*, vol. 40, no. 5, pp. 793–800, 2008.

[11] A. Arrigoni, C. Beckett, D. Ciancio, and G. Dotelli, "Life cycle analysis of environmental impact vs. durability of stabilised rammed earth," *Construction and Building Materials*, vol. 142, pp. 128–136, 2017.

[12] Q. B. Bui, J. C. Morel, B. V. V. Reddy, and W. Ghayad, "Durability of rammed earth walls exposed for 20 years to natural weathering," *Building and Environment*, vol. 44, no. 5, pp. 912–919, 2009.

[13] R. El-Nabouch, Q.-B. Bui, O. Plé, and P. Perrotin, "Assessing the in-plane seismic performance of rammed earth walls by

using horizontal loading tests," *Engineering Structures*, vol. 145, pp. 153–161, 2017.

[14] M. I. Gomes, M. Lopes, and J. Brito, "Seismic resistance of earth construction in Portugal," *Engineering Structures*, vol. 33, no. 3, pp. 932–941, 2011.

[15] Q.-B. Bui, S. Hans, J.-C. Morel, and A.-P. Do, "First exploratory study on dynamic characteristics of rammed earth buildings," *Engineering Structures*, vol. 33, no. 12, pp. 3690–3695, 2011.

[16] Q.-B. Bui, T.-T. Bui, and A. Limam, "Assessing the seismic performance of rammed earth walls by using discrete elements," *Cogent Engineering*, vol. 3, no. 1, article 1200835, 2016.

[17] T.-T. Bui, Q.-B. Bui, A. Limam, and J.-C. Morel, "Modeling rammed earth wall using discrete element method," *Continuum Mechanics and Thermodynamics*, vol. 28, no. 1–2, pp. 523–538, 2015.

[18] J. S. J. Cheah, P. Walker, A. Heath, and T. K. K. B. Morgan, "Evaluating shear test methods for stabilised rammed earth," *Proceedings of the Institution of Civil Engineers-Construction Materials*, vol. 165, no. 6, pp. 325–334, 2012.

[19] T.-T. Bui, Q.-B. Bui, A. Limam, and S. Maximilien, "Failure of rammed earth walls: from observations to quantifications," *Construction and Building Materials*, vol. 51, pp. 295–302, 2014.

[20] H. Nowamooz and C. Chazallon, "Finite element modelling of a rammed earth wall," *Construction and Building Materials*, vol. 25, no. 4, pp. 2112–2121, 2011.

[21] L. Miccoli, A. Drougkas, and U. Müller, "In-plane behaviour of rammed earth under cyclic loading: experimental testing and finite element modelling," *Engineering Structures*, vol. 125, pp. 144–152, 2016.

[22] L. Miccoli, D. V. Oliveira, R. A. Silva, U. Müller, and L. Schueremans, "Static behaviour of rammed earth: experimental testing and finite element modelling," *Materials and Structures*, vol. 48, no. 10, pp. 3443–3456, 2015.

[23] R. El-Nabouch, Q. B. Bui, O. Plé, and P. Perrotin, "Characterizing the shear parameters of rammed earth material by using a full-scale direct shear box," *Construction and Building Materials*, vol. 171, pp. 414–420, 2018.

[24] A. Arrigoni, A. C. Grillet, R. Pelosato et al., "Reduction of rammed earth's hygroscopic performance under stabilisation: an experimental investigation," *Building and Environment*, vol. 115, pp. 358–367, 2017.

[25] NF P94-093, Soils: reconnaissance et essais—Détermination des références de compactage d'un matériau—Essai Proctor Normal—Essai Proctor modifié, 2014..

[26] NF P 94-071-1. Sols: Reconnaissance et Essais—Essai de cisaillement rectiligne à la boîte—Partie 1: Cisaillement direct," AFNOR 08/1994..

[27] Q. B. Bui, S. Hans, and J. C. Morel, "The compressive strength and pseudo elastic modulus of rammed earth," in *Proceedings of the International Symposium on Earthen Structures*, pp. 217–223, Interline Publishers, Bangalore, India, August 2007.

[28] P. A. Jaquin, C. E. Augarde, D. Gallipoli, and D. G. Toll, "The strength of unstabilised rammed earth materials," *Géotechnique*, vol. 59, no. 5, pp. 487–490, 2009.

[29] P. Gerard, M. Mahdad, A. R. McCormack, and B. François, "A unified failure criterion for unstabilized rammed earth materials upon varying relative humidity conditions," *Construction and Building Materials*, vol. 95, pp. 437–447, 2015.

[30] NZS 4297, *Engineering Design of Earth Buildings*, New Zealand Standard, Auckland, New Zealand, 1998.

[31] A. Flitti, N. Della, and R. D. V. Flores, "Experimental study of the shear resistance of granular material: influence of initial state," *Journal of Theoretical and Applied Mechanics*, vol. 55, no. 2, pp. 523–533, 2017.

[32] R. Borja, *Plasticity-Modeling and Computation*, Verlag Berlin Heidelberg: Springer, Heidelberg, Germany, 2013.

[33] P. Vacher, S. Dumoulin, F. Morestin, and S. Mguil-Touchal, "Bidimensional strain measurement using digital images," *Proceedings of the Institution of Mechanical Engineers, Part C: Journal of Mechanical Engineering Science*, vol. 213, no. 8, pp. 811–817, 1999.

[34] Aster, *Analysis of Structures and Thermomechanics for Studies and Research*, EDF, Clamart, France, 2011, http://www.code-aster.org.

[35] R. El-Nabouch, *Mechanical behaviour of rammed earth walls under pushover tests*, Ph.D. thesis, Univ. Grenoble Alpes-Univ. Savoie Mont Blanc, Chambéry, France, 2017.